American Mineralogist, Volume 64, pages 1036–1048, 1979

The system $NaAlSi_3O_8$–H_2O–CO_2 to 20 kbar pressure: I. Compositional and thermodynamic relations of liquids and vapors coexisting with albite

DAVID H. EGGLER[1]

Geophysical Laboratory, Carnegie Institution of Washington
Washington, D.C. 20008
and Department of Geosciences, The Pennsylvania State University
University Park, Pennsylvania 16802

AND A. A. KADIK

V. I. Vernadsky Institute of Geochemistry and Analytical Chemistry, USSR
Academy of Sciences, Moscow

Abstract

The distribution of H_2O and CO_2 between liquid and vapor, in equilibrium with albite crystals, has been determined in eight isothermal, isobaric sections at pressures from 3 to 20 kbar. These data project into P–T space as melting curves at particular vapor compositions.

The H_2O contents of liquids that were determined experimentally and those calculated from the thermodynamic model of Burnham and Davis are in agreement, even at pressures to 20 kbar. Activity coefficients for H_2O in the CO_2–H_2O vapor [$\gamma(H_2O)^v$], calculated over the range 3–20 kbar and 900°–1100°C, are everywhere >1. Because of nonideal mixing in the vapor, melting curves appear at lower temperatures in P–T–$X(H_2O)^v$ projection than in P–T–$a(H_2O)^m$ projection (as calculated by Burnham). The mixing is least ideal [$\gamma(H_2O)^v$ is greatest] in the pressure range 5–10 kbar, resulting in a pronounced trough of temperature minima on the melting curves.

Introduction

Since the work of Goranson (1938), $NaAlSi_3O_8$ (albite) has been recognized as a useful synthetic composition for modeling of thermodynamic properties of silicate melts, in particular melts of granitic compositions. Phase-equilibrium and thermodynamic data on the join $NaAlSi_3O_8$–H_2O by Goranson (1938) and Burnham and Davis (1971, 1974) have been extended to the join $NaAlSi_3O_8$–H_2O–CO_2 in preliminary studies by Millhollen *et al.* (1971) and Eggler (1973). Sufficient experiments have now been conducted to characterize melting and solubility relations on the join to a pressure of 20 kbar.

The experiments have yielded a set of data, previously unavailable for any silicate, for the partitioning of CO_2 and H_2O between liquids and vapor. Because CO_2 and H_2O are considered to be the principal volatile constituents of the upper mantle (summarized by Eggler and Rosenhauer, 1978) and crust (Roedder, 1970; Sobolev *et al.*, 1970; Bazarova *et al.*, 1975; Touret, 1971), such a data set is essential for modeling of processes in which volatiles are involved. These processes—including anatexis (particularly in the lower crust), evolution of vapor from magmas, diapiric rise of magmas, and volatile evolution of the continental crust—will be discussed in the second part of this paper. This part is concerned with the experimental data and with a by-product of the research, activity coefficients of H_2O in H_2O–CO_2 vapor. Such coefficients should be useful for thermodynamic calculations in both metamorphic and igneous petrology.

Experimental data

Starting materials

Three albite starting materials were used: the same sample of Varütrask albite (Ab 98.7, Or 0.7, An 0.6

[1] Present address: Department of Geosciences, The Pennsylvania State University, University Park, Pennsylvania 16802.

0003-004X/79/0910-1036$02.00

mole percent) used by Kracek and Neuvonen (1952); albite glass prepared from oxides; and a mechanical mixture of Al_2O_3, SiO_2 (cristobalite), and Na_2CO_3.

Experimental techniques

Approximately 10 mg of prepared compositions were loaded into Pt capsules with H_2O and $Ag_2C_2O_4$, in the requisite proportions. The capsules were welded shut without loss of volatiles.

Runs from 3 to 10 kbar were made in an internally heated, argon-pressurized vessel (Yoder, 1950). Runs from 10 to 30 kbar were made in solid-media, high-pressure apparatus, using talc–boron nitride assemblies. For runs at 950°C, 20 kbar, a floating-piston technique was employed; for all other runs, the piston-out technique was used. The reported nominal pressures are accurate to within 2 percent, relative (Eggler, 1977). Temperature was measured with Pt–Pt90Rh10 thermocouples with no correction of the emf for pressure.

Analytical techniques

Phases in the run products were identified by optical examination. Quenching in solid-media apparatus was sufficiently rapid that liquid quenched unambiguously to glass, but in some runs in the gas-media apparatus, liquid quenched to glass and crystals of albite, which from their anhedral form and irregular extinction have been interpreted as quench crystals. Vapor quenched to low-birefringence material, to glass of refractive index different from quenched liquid, or in some experiments at 15–20 kbar (for bulk compositions close to the H_2O–CO_2 join), to material that included carbonate. Trapped inclusions of the vapor phase separated into two phases, H_2O-rich liquid and CO_2-rich gas.

The CO_2 content of quenched glasses from several runs was determined by β-track autoradiography (Mysen and Seitz, 1975); a portion of the C of the Na_2CO_3 in the mechanical mixture was ^{14}C.

Data

Critical runs are listed in Table 1. Almost all the data have been plotted in isothermal, isobaric sections, shown in Figures 1–3. These sections were chosen for experimental study in order to determine the distribution of CO_2 and H_2O between liquid and vapor. Phase boundaries were not reversed, but runs were made with different starting materials and for various lengths of time to test for equilibrium. It should be pointed out, moreover, that although a product of this study is a set of *solidus* curves, the bulk of the data has been obtained at *liquidus* temperatures. (This seemingly contradictory statement can be understood if the boundary between Ab + L + V and L + V in, for example, Fig. 1 is considered. This boundary is a liquidus boundary, but its intersection with the liquid-saturated vaporus determines the vapor composition at the solidus at the temperature and pressure of the section.) Not only are relations at liquidus curves determined with less ambiguity, but equilibrium is approached at faster rates.

Determination of the composition of vapor coexisting with liquid and albite is relatively simple. Runs in which liquid or albite is absent delineate the apex of the three-phase triangle Ab + L + V near the H_2O–CO_2 sideline (*e.g.*, Fig. 1). Determination of liquid composition is more difficult because it involves delineation of phase boundaries between vapor-present and vapor-absent assemblages, often a trying task because of problems in identifying quenched vapor. These difficulties have been overcome in this study by use of a new technique. The Ab + L side of the three-phase triangle Ab + L + V was located precisely by determining the CO_2 content of the melt, in runs quenched from the Ab + L + V field, by autoradiography. Because this tie line is approximately parallel to the Ab–H_2O sideline, and because the tie line L + V can be located precisely by runs (presence or absence of albite crystals), the composition of L is readily determined without recourse to determination of the presence or absence of vapor. Other studies (Mysen *et al.*, 1975; Mysen and Seitz, 1975) have shown that equilibrium concentrations of CO_2 can be quenched into glass. This conclusion was checked for albite–H_2O–CO_2 by determining the CO_2 content of liquid at 20 kbar and 950°C by two methods (Fig. 1). The boundary between Ab + L + V and Ab + L was first determined from the presence or absence of bubbles, enclosed within glass, containing quenched vapor material (see above). The CO_2 content of the liquid was thus fixed by phase equilibria at 5±3 mole percent CO_2, equivalent to 2.0 weight percent CO_2. [The molecular weight of liquid albite is taken as 262, as by Burnham and Davis (1971).] Then a run was made with the radioactive mix and H_2O, which contained as run products vapor, liquid, and a trace of crystals. Analysis of the glass showed 2.23±0.06 weight percent CO_2, or 6 mole percent, well within the error of the phase equilibria (5±3). Based on this successful test, in the determinations of other three-phase triangles (Figs. 2–3) the autoradiographic

Table 1. Results of critical quenching experiments in the system $NaAlSi_3O_8$–H_2O–CO_2

Composition of mix, wt %			Anhydrous starting materials	P, kbar	T, °C	Time, hr	Phases present
Ab	CO_2	H_2O					
89.9	7.5	2.6	M	3	850	21	Ab, *V*
48.4	36.6	15.0	Ab, Ag	3	850	20	Ab, *L*, *V*
49.1	34.7	16.2	Ab, Ag	3	850	17	Ab, *L*, *V*
49.9	32.6	17.5	Ab, Ag	3	850	17.5	Ab, *L*, *V*
50.6	30.6	18.8	Ab, Ag	3	850	28	*L*, *V*, Ab (quench)
51.4	28.5	20.1	Ab, Ag	3	850	28	*L*, *V*, Ab (quench)
89.3	7.5	3.2	M	3	850	20	Ab, *L* (trace), *V*
84.5	7.1	8.4	M	3	850	21	Ab, *L*, *V*
92	1.0	7.0	M, Ab	3	850	21	Ab, *L*, *V*
83	7.2	9.8	M	3	850	21	*L*, *V*
90.2	1.5	8.3	Ab, M	3	850	21	*L*, *V*
88.7	1.6	9.7	Ab, M	3	850	17	*L*, *V*, Ab (quench)
94.0	0.0	6.0	Ab	3	850	21	*L*, Ab
93.1	0.0	6.9	Ab	3	850	21	*L*, Ab (quench) ∿ 1%
43.2	50.8	6.0	Ab, Ag	7	850	21	Ab, *V*
43.8	44.3	6.9	Ab, Ag	7	850	20	Ab, *V*
91.3	7.7	1.0	M	7	850	20	Ab, *V*
44.6	41.1	8.3	Ab, Ag	7	850	17	Ab, *L*, *V*
45.4	44.9	9.7	M, Ag	7	850	21	Ab, *L*, *V*
46.2	42.7	11.1	M, Ag	7	850	18	*L*, *V*, Ab (quench)
84.8	7.1	8.1	M	7	850	21	Ab, *L*, *V*
83.6	7.0	9.4	M	7	850	20	*L*, *V*
91.4	1.0	7.6	Ab, M	7	850	21	*L*, *V*
85.3	1.6	10.1	Ab, M	7	850	20	*L*, *V*
92.8	0.0	7.2	Ab	7	850	20	*L*, Ab
92.3	0.0	7.7	Ab	7	850	18	*L*, Ab (quench)
90.7	0.0	9.3	Ab	7	850	18	*L*
60.9	37.8	1.3	Ab, Ag	7	950	19	Ab, *V*
61.6	36.3	2.1	Ag, Ab	7	950	17.5	Ab, *L*, *V*
62.4	34.6	3.0	Ag, Ab	7	950	17.3	Ab, *L*, *V*
63.2	32.9	3.9	Ag, M	7	950	21.75	Ab, *L*, *V*
87.9	7.4	4.7	M	7	950	19	Ab, *L*, *V*
92.3	1.7	6.0	Ab, M	7	950	19	Ab, *L*, *V*
34.3	58.3	7.4	Ag, M	7	950	17.5	*L*, *V*
63.8	31.6	4.6	Ag, M	7	950	21.75	*L*, *V*, Ab
64.8	29.4	5.8	Ag, M	7	950	21.75	*L*, *V*, Ab (quench)
87.2	7.3	5.5	M	7	950	21.75	*L*, *V*, Ab (quench)
86.3	7.2	6.5	M	7	950	17.5	*L*, *V*, Ab (quench)
84.8	7.3	7.9	M	7	950	17.5	*L*, *V*
93.6	0.0	6.4	Ab	7	950	17.5	*L*
94.7	0.0	5.3	Ab	7	950	17.5	Ab, *L*
60.9	37.8	1.3	Ag, Ab	7	1050	18	Ab, *L*, *V*
61.6	36.3	2.1	Ag, Ab	7	1050	18	Ab, *L*, *V*
62.4	34.6	3.0	Ag, Ab	7	1050	18	Ab, *L*, *V*
89.3	7.5	3.2	M	7	1050	18	Ab, *L*, *V*

method was used entirely; as a precaution, however, runs were selected for analysis that had compositions (within the Ab + L + V field) near the L field and that contained as products small amounts of stable crystals and no quench crystals.

Each three-phase triangle is in effect one determination of the composition of coexisting liquid and vapor and simultaneously of one P-T-$X(CO_2)^v$ point on the melting (solidus) surface of albite, where $X(CO_2) = CO_2/(CO_2 + H_2O)$ (mole). The data have been combined in three diagrams. Figure 4 shows the compositions of coexisting vapor and liquid, in terms of $X(CO_2)$, in equilibrium with albite. The eight P-T-X determinations of this study are shown as open boxes. Results of other workers, also shown, are in general agreement; the differences amount to no

Table 1. (continued)

Composition of mix, wt %			Anhydrous starting materials	P, kbar	T, °C	Time, hr	Phases present
Ab	CO_2	H_2O					
88.6	7.5	3.9	M	7	1050	18	Ab, *L*, *V*
91.9	3.9	4.2	M, Ab	7	1050	18	Ab, *L*, *V*
94.6	1.1	4.3	M, Ab	7	1050	21	*L*, *V*, Ab (quench)
63.2	32.9	3.9	Ag, M	7	1050	20.5	*L*, *V*
63.8	31.6	4.6	Ag, M	7	1050	20.5	*L*, *V*
97.1	0.0	2.9	Ab	7	1050	20.5	Ab, *L*
96.7	0.0	3.3	Ab	7	1050	20.5	*L*
92.3	7.7	0.0	M	10	1240	4	Ab, *L*, *V*
92.3	7.7	0.0	M	10	1255	4	*L*, *V*
36.2	53.6	10.2	Ag, M	15	850	4	Ab, *V*
39.7	49.1	11.2	Ag, M	15	850	4	Ab, *L*, *V*
89.6	7.5	2.9	M	15	850	4	Ab, *L*, *V*
81.5	6.9	11.6	M	15	850	4	Ab, *L*, *V*
79.5	6.9	13.6	M	15	850	4	*L*, *V*, Ab (quench) << 1%
59.9	31.4	8.7	Ag, M	15	950	4	Ab, *L*, *V*
84.4	7.5	8.1	M	15	950	4	Ab, *L*, *V*
83.6	7.0	9.4	M	15	950	4	*L*, *V*
45.1	45.5	9.3	Ag, M	15	950	4	*L*, *V*
92.3	7.7	0.0	M	15	1260	1.5	Ab, *L*, *V*
92.3	7.7	0.0	M	15	1280	1	*L*, *V*
85.0	0.0	15.0	Gl, Ag	20	950	3	*L*
88.8	0.0	11.2	Gl, Ag	20	950	4	*L*
91.8	0.0	8.2	Gl, Ag	20	950	4	*L*, Ab (sa)
80.8	10.2	9.0	Gl, Ag	20	950	5	*L*, *V*, Ab (sa)
42.7	51.6	5.7	Gl, Ag	20	950	4	Ab
82.3	6.4	11.3	Gl, Ag	20	950	5	*L*, *V* (rare)
88.2	2.6	9.2	Gl, Ag	20	950	10	*L*, *V* (sa)
86.5	4.1	9.4	Gl, Ag	20	950	5	*L*, *V* (sa)
37.6	51.1	11.3	Gl, Ag	20	950	4	*L*, *V*
90.6	1.2	8.2	Gl, Ag	20	950	5	*L*, Ab (sa)
89.2	2.7	8.1	Gl, Ag	20	950	5	*L*, Ab (sa), *V* (rare)
43.7	48.8	7.5	Gl, Ag	20	950	3	*L*, Ab, *V*
70.8	21.2	8.0	Gl, Ag	20	950	4	*L*, Ab (sa), *V*
84.3	7.1	8.7	M	20	950	5	*L*, *V*
43.8	49.3	6.9	Ag, M	20	1050	4	Ab, *L*, *V*
85.3	7.1	7.5	M	20	1050	3	Ab, *L*, *V*
61.7	29.8	8.5	Ag, M	20	1050	4	*L*, *V*
84.5	7.1	8.4	M	20	1050	4	*L*, *V*
92.3	7.7	0.0	M	20	1200	2	Ab, *L*, *V*
92.3	7.7	0.0	M	20	1275	1.5	Ab, *L*, *V*
92.3	7.7	0.0	M	30	1374	0.8	Ab, *L*, *V*
92.3	7.7	0.0	M	30	1400	0.8	*L*, *V*

Abbreviations: (1) Starting materials: M, oxide-carbonate mix; Ab, crystalline albite; Gl, albite glass; Ag, $Ag_2C_2O_4$. (2) Run products: Ab, albite crystals; *L*, quenched liquid (glass); quench, albite crystals interpreted to have quenched from liquid; *V*, quenched vapor; sa, small amount.

more than 50°C, the larger deviations occurring in the low-pressure region where the curves change most rapidly and where small uncertainties in pressure or composition produce large apparent errors in temperature.

The smoothed vapor curves from Figure 4 have been used to plot solidus curves in P-T projection in Figure 5. Brackets at temperatures above 1050°C were estimated by smoothly connecting the solidus curve at each pressure, below 1050°C, to the melting curve in the presence of CO_2. The runs used to bracket that melting curve of albite in the presence of

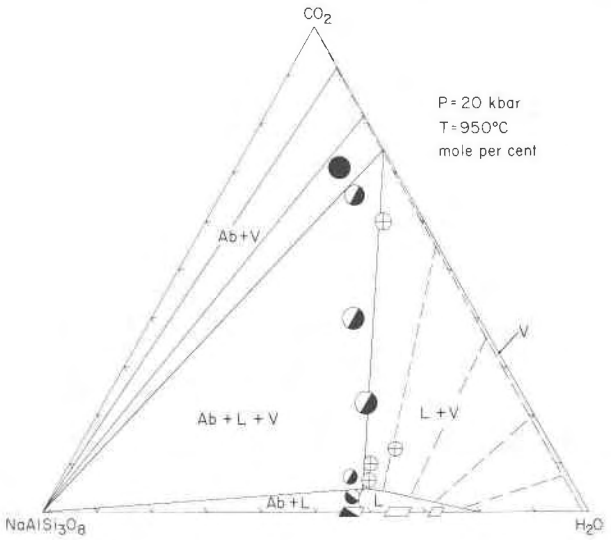

Fig. 1. Isobaric, isothermal section of the join $NaAlSi_3O_8$–CO_2–H_2O at 20 kbar. Compositions are in mole percent. The CO_2 content of liquid coexisting with albite and vapor has been determined both by phase equilibria (shown) and by autoradiography of a glass quenched from the Ab + L + V field.

CO_2 are also shown in Figure 5. If the CO_2 were pure, albite would melt completely at one temperature. The CO_2 is not pure, however, containing about 1 mole percent CO and 1 mole percent H_2O produced by H_2 diffusion from the assembly (Eggler *et al.,* 1974). Because of these impurities in the vapor phase, a divariant melting interval is developed between the solidus and the liquidus. This interval was found to be 100°C or more. Because the liquidus temperature in the system diopside–CO_2 for $X(CO_2)^v \approx 0.98$ is within 10°C of the liquidus (hence solidus) temperature for $X(CO_2)^v = 1.0$ (Eggler, 1973), the analogous liquidus curve for albite for $X(CO_2)^v \approx 0.98$ can be assumed to be very near the liquidus curve for $X(CO_2)^v = 1.0$. The curve for $X(CO_2)^v \approx 0.98$ is in fact close to the volatile-absent melting curve, as determined by Boyd and England (1963). (The volatile-absent curve was checked by melting synthetic albite at 10 kbar pressure; the temperature obtained agreed within 10°C with the curve of Boyd and England, 1963.) The very small freezing-point depression is further evidence of the low solubility of CO_2 in albite melt.

The contents of CO_2 and H_2O in liquids in equilibrium with crystals and vapor are shown in Table 2 and Figure 6. The CO_2 contents were determined by autoradiography, whereas the H_2O contents were taken from phase diagrams (Figs. 1–3). Temperatures and compositions of the coexisting vapor phase along the polythermal saturation surfaces in Figure 6 are easily read from Figure 4.

Discussion

The principal discoveries in this study are that there is a pronounced trough of temperature minima on the CO_2/H_2O divariant melting surface at a pressure of approximately 8 kbar (Fig. 5) and that, even though H_2O is always strongly partitioned into albite liquid in preference to CO_2 (Fig. 4), the partitioning changes with P and T. The minimum trough, predicted theoretically by Sobolev *et al.* (1970), is defined by strongly negative slopes of melting curves at low $X(H_2O)^v$ between 0 and 8 kbar and strongly positive slopes between 8 and 20 kbar. The same type of trough has been found in melting curves in the system diopside–H_2O–CO_2 (Eggler and Rosenhauer, 1978). There is also a trough in the P-T-$a(H_2O)^m$ curves in the system albite–H_2O (without CO_2) at 1–4 kbar (Burnham, 1979, Fig. 16-6), but that trough is shallower and occurs at lower pressures. In other words, slopes of melting curves are less negative at low pressures and less positive at high pressures. For instance, the curve at $X(H_2O)^v = 0.2$ between 10 and 20 kbar has a slope of 10°C/kbar in diopside–H_2O–CO_2 and 12°C/kbar in albite–H_2O–CO_2, whereas an approximately equivalent curve in albite–H_2O at $a(H_2O)^m = 0.5$ has a slope of 5°C/kbar.

Other findings confirm previous experimental discoveries. These findings include low but finite CO_2 solubilities in albite melt (Eggler, 1973; Mysen *et al.,* 1975), maxima of CO_2 solubility on polythermal vapor-saturation surfaces (*e.g.,* Fig. 6; Eggler, 1973; Mysen, 1976), and divariant solidus surfaces in the presence of CO_2 and H_2O (*e.g.,* Fig. 5 and Millhollen, 1971).

Thermodynamic calculations

Activity of H_2O in albite liquid

The equation expressing equilibrium between pure crystalline albite and albite liquid containing dissolved H_2O and CO_2 is (Burnham, 1979, eq. 16-12)

$$\mu(\text{ab})^m - \mu(\text{ab})^s = 0 = \Delta G^\circ(m\text{ab}) + P\Delta V(m\text{ab}) + RT\ln a(\text{ab})^m \quad (1)$$

where $a(\text{ab})^m$ is the activity of $NaAlSi_3O_8$ in the liquid relative to pure $NaAlSi_3O_8$ liquid at P and T (°K), ΔG° ($m$ab) is the free energy of fusion of albite at T and 1 bar (Robie and Waldbaum, 1968), and $\Delta V(m)$ is the average volume change (187 cal/kbar;

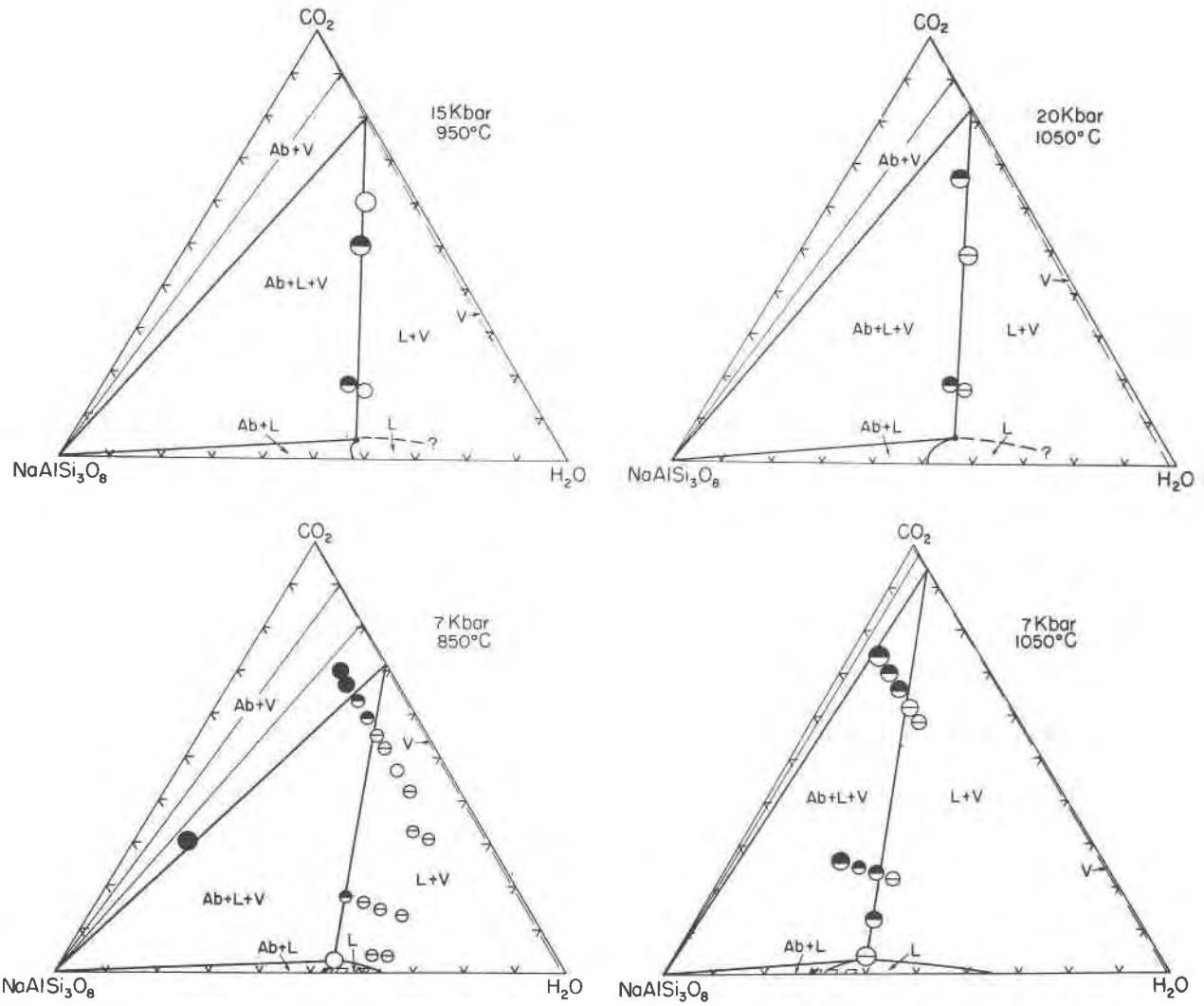

Fig. 2. Isobaric, isothermal sections of the join $NaAlSi_3O_8$–CO_2–H_2O. Compositions are in mole percent. Sizes of the run symbols indicate the uncertainties (due to weighing errors) in the compositions. The CO_2 contents of liquids coexisting with albite and vapors were determined by autoradiography of glasses quenched from the Ab + L + V field. Triangle indicates a H_2O solubility determined by Burnham and Davis (1974).

Burnham, 1979). Because CO_2 and H_2O dissolve in silicate liquids by different mechanisms, it is necessary to separate the effects of the two volatiles on $a(\text{ab})^m$. For small values of $X(CO_2)^m$ [large values of $X(\text{ab})^m$], it can be assumed that liquids in the system $NaAlSi_3O_8$–CO_2 obey Raoult's law and that

$$a(\text{ab})^m = 1 - X(CO_2)^m \qquad (2)$$

This assumption can be checked by comparison of the depression of the solidus calculated to be due to solution of CO_2 with the depression determined by experiment. A representative case is the solidus at 15 kbar. The depression at 15 kbar, calculated from (1) and (2), is 18°C. The experimentally determined depression at 15 kbar (Fig. 5) is 10°±10°C. The agreement is sufficiently close and the effect sufficiently small to warrant use of the Raoultian model. The relations between $X(H_2O)^m$ and $a(H_2O)^m$, derived by Burnham (1979, eqs. 16-13 and 16-14), can be combined with (1) and (2) to yield, for $X(H_2O)^m > 0.5$:

$$\ln[1 - X(H_2O)^m] + X(H_2O)^m = \{0.252T + 1023 - \Delta G^\circ(m\text{ab}) - P\Delta V(m\text{ab}) - RT\ln[1 - X(CO_2)^m]\}/(12.96T - 5300) \qquad (3)$$

and for $X(H_2O)^m \leq 0.5$:

$$\ln[1 - X(H_2O)^m] =$$

$$-\left[\frac{\Delta G^\circ(mab) + P\Delta V(mab)}{2RT}\right] - \frac{1}{2}\ln[1 - X(CO_2)^m] \quad (4)$$

The $a(H_2O)^m$ can be calculated readily for $X(H_2O)^m \leq 0.5$ (Burnham, 1979):

$$a(H_2O)^m = k[X(H_2O)^m]^2 \quad (5)$$

or for $X(H_2O)^m > 0.5$ from

$$a(H_2O)^m = 0.25\, k \exp\{(6.52 - 2667/T)[X(H_2O)^m - 0.5]\} \quad (6)$$

and values of k from Burnham (1979, Fig. 16-3).

Values of $X(H_2O)^m$ have been calculated from (3) or (4) at the P and T of the eight experimentally determined three-phase triangles as well as at two other P,T coordinates (Table 2). The calculated $X(H_2O)^m$ can be compared with the experimentally determined $X(H_2O)^m$ (column 6, where values and uncertainties are estimated from Figs. 1–3) and with two values of $X(H_2O)^m$ that can be confidently interpolated from Figures 4 and 6. The agreement is close with two exceptions: the calculated $X(H_2O)^m$ at 20 kbar, 950°C, is higher than the experimental value, whereas the calculated $X(H_2O)^m$ at 7 kbar, 1050°C, is lower. In

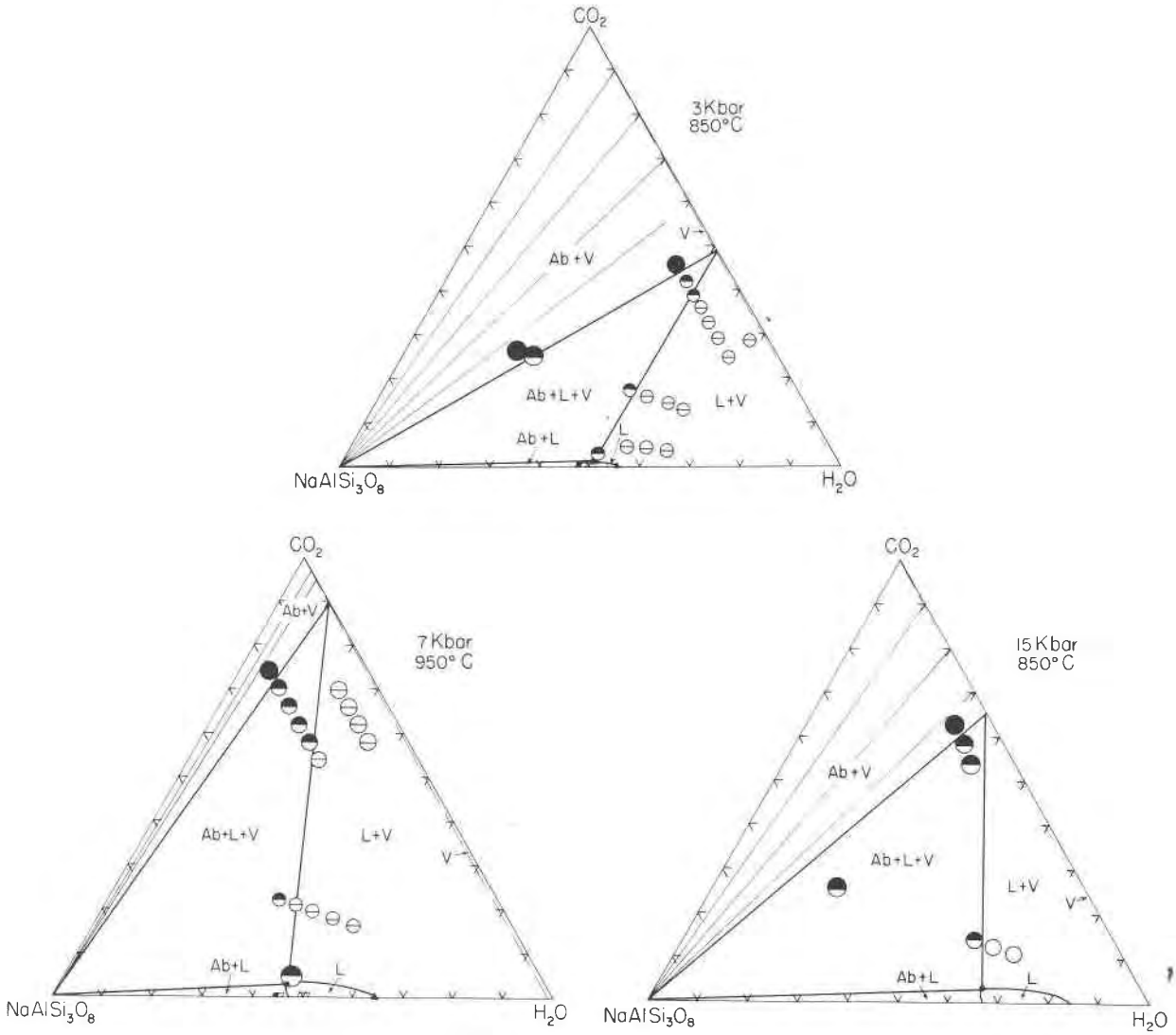

Fig. 3. Isobaric, isothermal sections of the join $NaAlSi_3O_8$–CO_2–H_2O. Compositions are in mole percent. Sizes of the run symbols indicate the uncertainties (due to weighing errors) in the compositions. The CO_2 contents of liquids coexisting with albite and vapors were determined by autoradiography of glasses quenched from the Ab + L + V field. Triangles indicate H_2O solubilities determined by Burnham and Davis (1974).

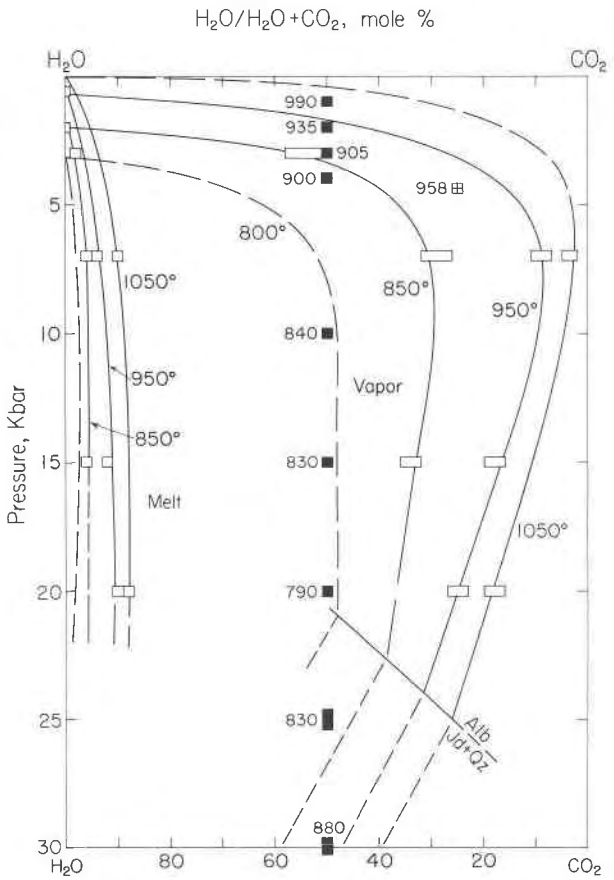

Fig. 4. Compositions, in mole percent, of volatile content of vapor and melt in equilibrium with albite. Points denoted by open boxes have been determined in isothermal, isobaric sections. Points denoted by closed boxes were determined by Millhollen *et al.* (1971) at the temperatures indicated. Point denoted by cross in box was determined by Kesson and Holloway (1974).

neither case is the calculated value more than 0.04 outside the experimental range of uncertainty. The close agreement indicates that the data of Burnham and Davis (1974) can be extended to liquids containing small amounts of CO_2 at pressures of at least 20 kbar.

Activity of H_2O in CO_2-H_2O vapor

Values of $a(H_2O)^m$, calculated from the calculated $X(H_2O)^m$ and (5) or (6), are listed in Table 2. Also listed are the experimental $X(H_2O)^v$ (Figs. 1–3), with two values of $X(H_2O)^v$ interpolated from Figure 4. The uncertainties include possible errors in pressure and temperature (Fig. 4) as well as phase boundaries (Figs. 1–3). Because $a(H_2O)^m = a(H_2O)^v$ and $\gamma(H_2O)^v = a(H_2O)^v/X(H_2O)^v$, $\gamma(H_2O)^v$ is readily calculated. It is assumed in calculating $X(H_2O)^v$ that vapors are essentially binary H_2O–CO_2 solutions, containing negligible amounts of Na_2O, Al_2O_3, and SiO_2. Burnham (in Clark, 1966, p. 436) found that the mole fraction of $NaAlSi_3O_8$ in the aqueous phase in equilibrium with albite melt at 7 kbar and 750°C is only 0.004. Although this amount would increase with pressure, Burnham (1979) has also found that the assumption of zero solubility of albite in H_2O vapor introduces negligible error in thermodynamic calculations even at 15 kbar. The vapors considered here, moreover, are not H_2O, but H_2O–CO_2; Eggler and Rosenhauer (1978) have shown that silicates are considerably less soluble in H_2O–CO_2 vapor than in H_2O vapor. The uncertainties in $\gamma(H_2O)^v$ listed include uncertainties in the terms $\Delta G°(mab)$, RT ln$[1 - X(CO_2)^m]$, and $X(H_2O)^v$. It can be shown from calculation of the H_2O-saturated solidus of albite that the uncertainty in $\Delta G°$ (mab) is less than 100 cal. Uncertainties in RT ln$[1 - X(CO_2)^m]$, allowing a generous ±100 percent in the estimated $X(CO_2)^m$, are also less than 100 cal. Errors of 100 cal change a calculated $X(H_2O)^m$ by only about 0.005 and $a(H_2O)^m$ by about 0.01, causing negligible uncertainty in a calculated value of $\gamma(H_2O)^v$. The term that is principally contributive to uncertainty in $\gamma(H_2O)^v$ is the measured $X(H_2O)^v$.

Values of $\gamma(H_2O)^v$ from Table 2 at 7, 15, and 20 kbar are plotted in Figure 7, together with other values calculated from the smoothed curves in Figure 4 or 5. In calculation of these other values, the procedure described above was iterated in order to obtain a value of $X(CO_2)^m$ from the curves in Figure 6.

Although the albite–H_2O–CO_2 melting curves cover a range of temperatures (Fig. 5), it is not possible to extract information on the temperature-dependence of γ from the data, because isobars cross the melting curves only once (Fig. 5). Chou and Williams (1977) have determined $\gamma(H_2O)^v$ at 4–8 kbar and 600°C, however, by a hydrogen fugacity sensor technique. Values at 3 and 7 kbar and 600°C, interpolated from their data, can be compared with data at higher temperatures from this study (Fig. 8). The data from this study were taken from Figure 7 and from a similar curve at 3 kbar. Although it may seem naïve to connect the sets of data with straight lines, these lines, when extrapolated into the region 1200°–1400°C, pass precisely through the points obtained by Eggler and Burnham (1978) from thermodynamic analysis of melting curves in the system $CaMgSi_2O_6$–CO_2–H_2O. The lines at 20 kbar (Fig. 8) were actually drawn between data of this study and data of Eggler and Burnham (1978), but they could have been

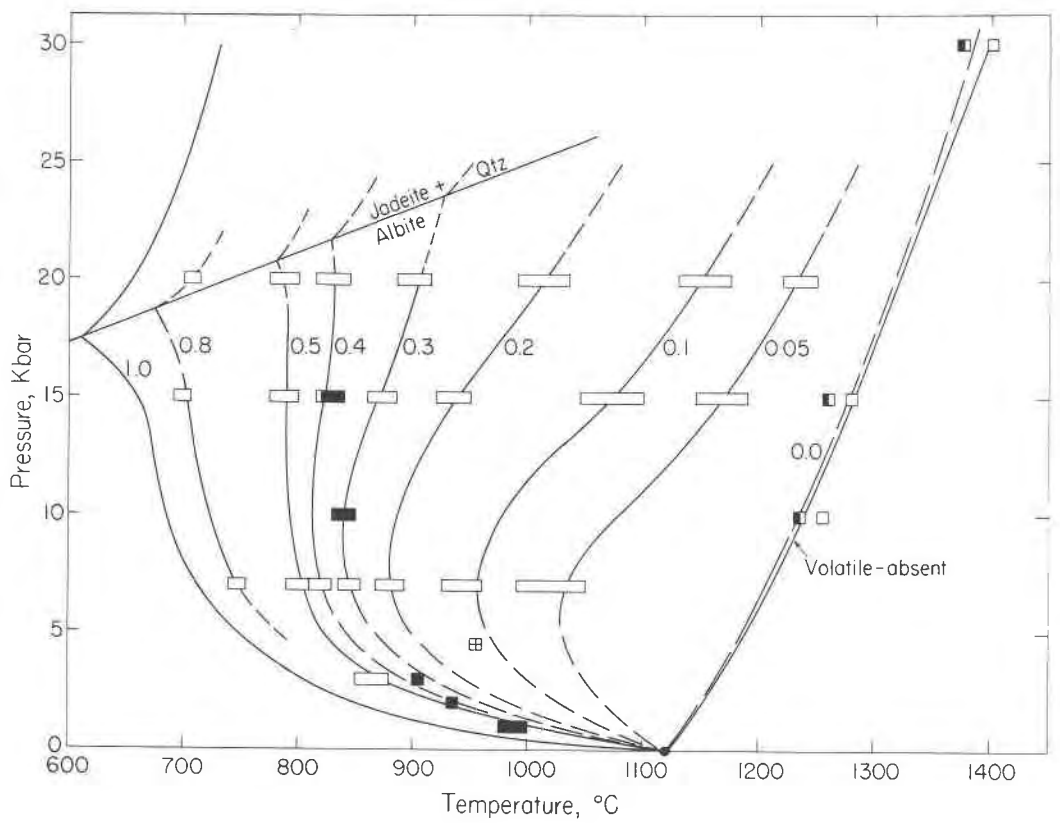

Fig. 5. Melting (solidus) curves of albite as a function of vapor composition [$X(H_2O)^v$, mole]. Open boxes are data of this report. Closed boxes are data from Millhollen *et al.* (1971), $X(H_2O)^v = 0.5$; cross in box, from Kesson and Holloway (1974), $X(H_2O)^v = 0.25$. Volatile-absent melting curve is from Boyd and England (1963). Run symbols delimit the CO_2-saturated melting curve. Albite = jadeite + quartz transition is from Boettcher and Wyllie (1968).

Table 2. Experimentally determined CO_2 and H_2O contents of liquid and vapor in equilibrium with albite crystals, and calculated activities of H_2O

		Liquid						Vapor	
P, kbar	T, °C	CO_2,* wt %	H_2O, wt %	CO_2, mole %	H_2O, mole %	H_2O, mole % calc.**	$a(H_2O)^m$, calc.**	$X(H_2O)^V$, mole	$\gamma(H_2O)^V$, calc.
3	850	0.32 ± 0.02	6.4	1.0	50 ± 3	49.9	0.81	0.51 ± 0.04	1.59 ± 0.12
7	850	0.86 ± 0.05	7.4	3.0	53 ± 4	56.5	0.69	0.28 ± 0.04	2.5 ± 0.3
7	950	0.88 ± 0.04	5.6	2.9	45 ± 4	44.6	0.42	0.10 ± 0.03	4.2 ± 1.0
7	1050	0.95 ± 0.07	4.2	3.5	38 ± 4	30.4	0.20	0.05 ± 0.03	4.0 ± 1.5
15	850	1.60 ± 0.05	12.2	3.5	65 ± 4	66.5	0.67	0.35 ± 0.04	1.91 ± 0.20
15	950	1.80 ± 0.08	8.9	4.8	55 ± 5	57.6	0.48	0.20 ± 0.04	2.4 ± 0.4
15	1050	1.60***	6.0***	5.0***	45***	47.2	0.31	0.11***	2.8 ± 0.6
20	850	1.80***	14.4***	3.5***	69***	71.0	0.71	0.36***	1.97 ± 0.19
20	950	2.23 ± 0.05	9.0	6.0	56 ± 4	63.1	0.53	0.25 ± 0.04	2.1 ± 0.3
20	1050	2.20 ± 0.13	7.8	6.0	53 ± 5	54.7	0.37	0.18 ± 0.04	2.1 ± 0.4

*Determined by autoradiography of quenched glass.
**Calculated from data of Burnham and Davis (1974).
***Interpolated from Figures 4 and 6.

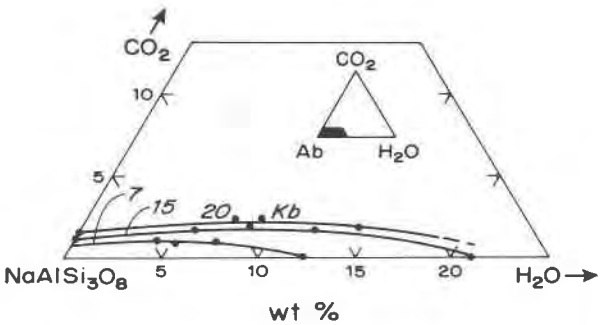

Fig. 6. Isobaric, polythermal vapor saturation curves of liquid in equilibrium with vapor and albite. Compositions are in weight percent. Data points are from Table 2; the H_2O-free and CO_2-free saturation values are from Mysen *et al.* (1975) and Burnham and Davis (1974).

drawn, at least roughly, by extrapolating the slopes at 3, 5 (not shown), and 7 kbar (Fig. 8) to higher pressures.

Points along isotherms from Figure 8 and points from similar diagrams (not shown) at 5, 10, and 15 kbar can be replotted as curves of constant vapor

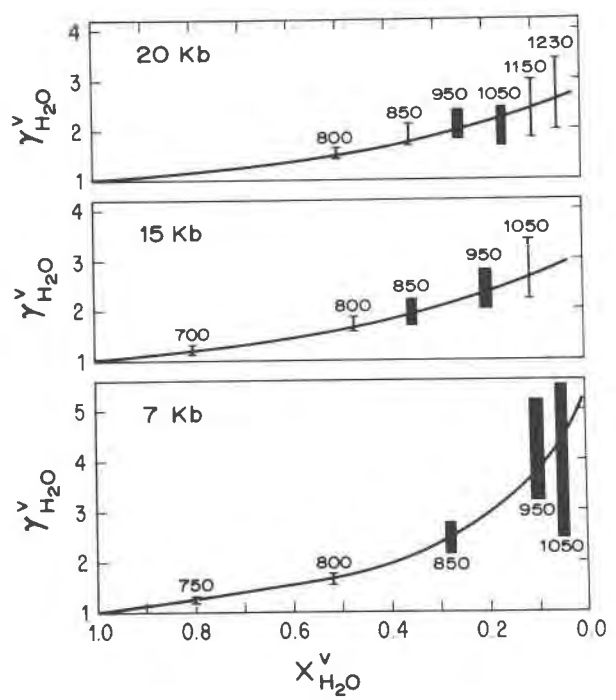

Fig. 7. Calculated activity coefficients of H_2O in a H_2O–CO_2 vapor phase. Brackets indicate the estimated ranges of uncertainty at each $X(H_2O)^v$. Values of $X(H_2O)^v$ for shaded brackets were determined in isothermal, isobaric sections; values for open brackets were interpolated from Fig. 4. Numbers next to each bracket indicate the temperatures (°C) at which the data were taken.

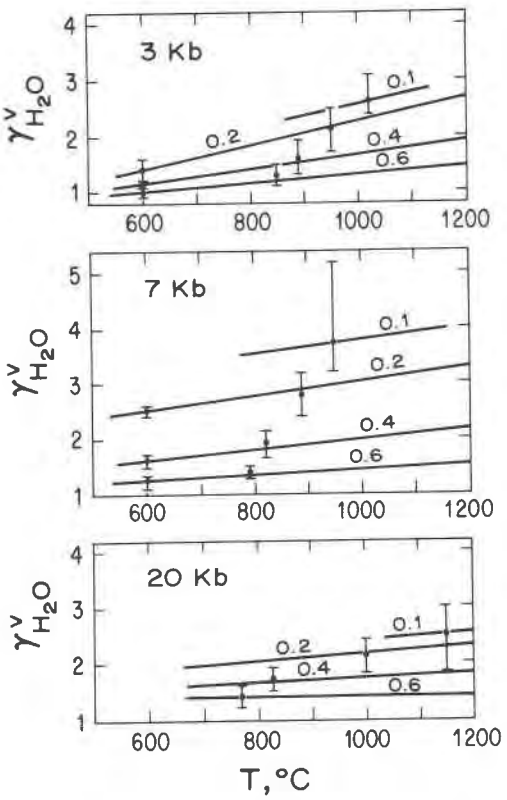

Fig. 8. Variation in $\gamma(H_2O)^v$ with temperature. Numbers next to each curve indicate $X(H_2O)^v$. The points shown at 600°C are from Chou and Williams (1977). The points shown at higher temperatures and the associated uncertainties have been replotted from Fig. 7 (this study).

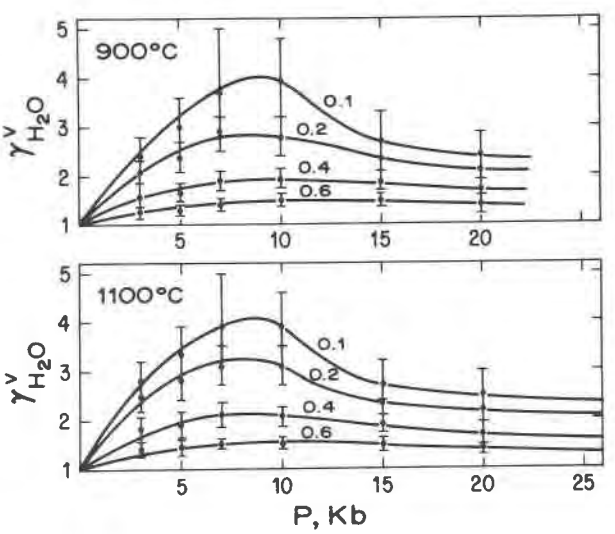

Fig. 9. Variations in $\gamma(H_2O)^v$ with pressure. Numbers next to each curve indicate $X(H_2O)^v$. The points shown and the associated uncertainties have been replotted from Fig. 8.

composition (Fig. 9). Such curves show the pressure-dependence of $\gamma(H_2O)^v$. Even allowing for the relatively large uncertainties in $\gamma(H_2O)^v$ at low $X(H_2O)^v$, it is apparent that there are maxima in $\gamma(H_2O)^v$ in the region 5–10 kbar. Maxima also occur in similar curves, at somewhat higher temperatures, calculated from melting relations in the system $CaMgSi_2O_6$–CO_2–H_2O (Eggler and Burnham, 1978).

Because the effects of temperature and pressure on $\gamma(H_2O)^v$ can be expected to be opposite, the occurrence of maxima in Figure 9 implies that minima ought to occur in Figure 8. The lines shown in Figure 8 are not inconsistent with that hypothesis, because at some temperature below 600°C, $\gamma(H_2O)^v$ must increase with decreasing temperature, inasmuch as temperatures are approaching the H_2O–CO_2 two-phase region.

The activity coefficients shown in Figures 8 and 9 can be applied, of course, in thermodynamic calculations involving CO_2–H_2O vapors in equilibrium with any silicate minerals or silicate liquids. Unfortunately, at present only one test of the data represented by Figures 8 and 9 can be made, under conditions somewhat beyond the experimentally determined pressure range. If the curves at 1100°C in Figure 9 are extrapolated to 26 kbar, the values of $\gamma(H_2O)^v$ at 26 kbar and 1100°C can be integrated, using the Gibbs–Duhem relation, to obtain $\gamma(CO_2)^v$. This integration, over the range $X(H_2O)^v = 0.0$–0.7, yields $\gamma(CO_2)^v = 1.70$ at $X(H_2O)^v = 0.7$. The $\gamma(CO_2)^v$ under the same conditions has been determined, from a decarbonation equilibrium (Eggler *et al.*, 1979), to be 1.60±0.14. This agreement is encouraging, but further independent determinations of activity coefficients are desirable, especially in the P–T regions where maxima occur.[2]

Slopes of melting curves: implications for $\gamma(H_2O)^v$

It was mentioned above in passing that slopes of the melting curves of albite (Figs. 4 and 5) are consistent with the calculations of $\gamma(H_2O)^v$. These relationships can be derived explicitly from expressions involving the chemical potentials of albite in the liquid and in crystalline albite:

$$d\mu(\mathrm{ab})^m = \left[\frac{\partial \mu(\mathrm{ab})^m}{\partial P}\right]_{T,X(\mathrm{ab})^m} dP + \left[\frac{\partial \mu(\mathrm{ab})^m}{\partial T}\right]_{P,X(\mathrm{ab})^m} dT + \left[\frac{\partial \mu(\mathrm{ab})^m}{\partial X(\mathrm{ab})^m}\right]_{T,P} dX(\mathrm{ab})^m \quad (7)$$

or

$$d\mu(\mathrm{ab})^m = \overline{V}(\mathrm{ab})^m dP - \overline{S}(\mathrm{ab})^m dT + RT\left[\frac{\partial \ln a(\mathrm{ab})^m}{\partial X(\mathrm{ab})^m}\right]_{T,P} dX(\mathrm{ab})^m \quad (8)$$

and

$$d\mu(\mathrm{ab})^s = V(\mathrm{ab})^s dP - S(\mathrm{ab})^s dT \quad (9)$$

Because $d\mu(\mathrm{ab})^m = d\mu(\mathrm{ab})^s$, (9) may be subtracted from (8) to yield

$$0 = \Delta\overline{V}(m\mathrm{ab})dP - \Delta\overline{S}(m\mathrm{ab})dT + RT\left[\frac{\partial \ln a(\mathrm{ab})^m}{\partial X(\mathrm{ab})^m}\right]_{T,P} dX(\mathrm{ab})^m \quad (10)$$

Because the melting curves of interest are those at the higher $X(CO_2)^v$, in the remaining discussion only values of $X(H_2O)^m \leq 0.5$ will be considered. In these cases, from (5):

$$\ln a(H_2O)^m = \ln k + 2 \ln X(H_2O)^m \quad (11)$$

and

$$X(H_2O)^m = \left[\frac{\gamma(H_2O)^v X(H_2O)^v}{k}\right]^{1/2} \quad (12)$$

From (11) and the Gibbs–Duhem relation,

$$\left[\frac{\partial \ln a(\mathrm{ab})^m}{\partial X(\mathrm{ab})^m}\right]_{T,P} = \frac{2}{X(\mathrm{ab})^m} \quad (13)$$

and from (12),

$$dX(H_2O)^m = \frac{X(H_2O)^m}{2}\left[d\ln\gamma(H_2O)^v - d\ln k\right] \quad (14)$$

For small $X(CO_2)^m$,

$$dX(\mathrm{ab})^m = -dX(H_2O)^m \quad (15)$$

and substituting (13) and (14) in (10) and rear-

[2] Comparison can be made to coefficients calculated from equations of state, such as the modified Redlich–Kwong (MRK) (Holloway, 1977). This comparison is not encouraging. The MRK coefficients are lower by 30–70 percent than the values in Table 2, the larger deviations occurring at smaller $X(H_2O)^v$. Unlike Figure 8, the temperature-dependence of MRK coefficients is slightly negative, and unlike Figure 9, maxima do not occur on isotherms.

ranging,

$$\left.\frac{dT}{dP}\right|_{X(H_2O)^v} = \frac{\Delta\bar{V}(mab) - \dfrac{RT\,X(H_2O)^m}{X(ab)^m}\left[\dfrac{d\ln\gamma(H_2O)^v}{dP} - \dfrac{d\ln k}{dP}\right]}{\Delta\bar{S}(mab)} \quad (16)$$

From (5), the following relation can also be derived:

$$dX(H_2O)^m = d\left[\frac{X(H_2O)^v\gamma(H_2O)^v}{k}\right] \Big/ 2X(H_2O)^m \quad (17)$$

Substituting (13), (15), and (17) in (10) and rearranging,

$$\left.\frac{dX(H_2O)^v}{dP}\right|_T = \frac{\Delta\bar{V}(mab) - \dfrac{RT\,X(H_2O)^m}{X(ab)^m}\left[\dfrac{d\ln\gamma(H_2O)^v}{dP} - \dfrac{d\ln k}{dP}\right]}{[RT\,\gamma(H_2O)^v]/[X(ab)^m X(H_2O)^m k]} \quad (18)$$

Extrema will be reached on melting curves, in the case of P–T projection, when (16) equals 0 and, in the case of P–X projection, when (18) equals 0. Because the numerators of (16) and (18) are the same, it will be appreciated that extrema occur under the same P–T–X conditions in Figures 4 and 5.

It can also now be appreciated why slopes of melting curves are consistent with the calculations of $\gamma(H_2O)^v$. As developed in the preceding section, melting curves in the system albite–H_2O–CO_2, contoured for $X(H_2O)^v$, do not fall at the same P–T coordinates as the melting curves in albite–H_2O, contoured for $a(H_2O)^m$. A small part of the differences is due to solution of CO_2 in the liquid, but most of the differences are due to nonideal mixing of H_2O and CO_2 in the vapor [$\gamma(H_2O)^v > 1$]. Of equal importance to the position of the curves, however, is their slope. If $\gamma(H_2O)^v$ were >1 but did not vary with P and T, so that $d\ln\gamma(H_2O)^v/dP = 0$, equation (16) shows that the dT/dP slopes of melting curves in albite–H_2O–CO_2 would be nearly the same as slopes in albite–H_2O, inasmuch as the remaining terms in (16), involving the liquid, are affected to a very small extent by solution of CO_2 in the liquid. These slopes would presumably become vertical at about 3 kbar, reflecting the shallow trough in the melting curves for albite–H_2O. Slopes of melting curves in albite–H_2O–CO_2 (Fig. 5) are not the same as in albite–H_2O (Burnham and Davis, 1974, Fig. 19; Burnham, 1979, Fig. 16–6), however, particularly at the lower $X(H_2O)^v$—they are distinctly less negative at low pressures and less positive at high pressures. As discussed above, these differences cannot originate from any term in equation (16) except the term $d\ln\gamma(H_2O)^v/dP$; this term must be positive at low pressures and negative at high pressures. In effect, this term deepens the shallow trough found in the albite–H_2O melting curves into the distinct trough found in the albite–H_2O–CO_2 curves. Stated differently, $\gamma(H_2O)^v$ must reach a maximum at some intermediate pressure. This conclusion, not surprisingly, is the same as that reached in the preceding thermodynamic analysis.

Acknowledgments

This research was supported in part by the NSF Earth Sciences Section, grants DES73-00266A01 and EAR77-15704. A. A. Kadik wishes to acknowledge the support and assistance of the National Academy of Sciences (United States) and of the Carnegie Institution of Washington in making possible his research at the Geophysical Laboratory.

Derivation of the thermodynamic relations and calculation of the thermodynamic variables were greatly facilitated through suggestions of C. Wayne Burnham. The manuscript was reviewed by C. Wayne Burnham, J. R. Holloway, D. R. Rumble, and H. S. Yoder, Jr.

References

Bazarova, T. Yu., J. T. Bakumenko, V. O. Kostyuk, L. I. Panina, V. S. Sobolev and A. I. Chepunov (1975) *Magmatic Crystallization as Based on the Study of Melt in Inclusions.* Publishing House Nauka, Siberian Branch, Novosibirsk (in Russian).

Boettcher, A. L. and P. J. Wyllie (1968) Jadeite stability measured in the presence of silicate liquids in the system $NaAlSiO_4$–SiO_2–H_2O. *Geochim. Cosmochim. Acta, 32,* 999–1012.

Boyd, F. R. and J. L. England (1963) Effect of pressure on the melting of diopside, $CaMgSi_2O_6$, and albite, $NaAlSi_3O_8$, in the range up to 50 kbar. *J. Geophys. Res., 68,* 311–323.

Burnham, C. W. (1979) The importance of volatile constituents. In H. S. Yoder, Jr., Ed., *The Evolution of the Igneous Rocks: Fiftieth Anniversary Appraisal,* p. 439–482. Princeton University Press, Princeton, New Jersey.

——— and N. F. Davis (1971) The role of H_2O in silicate melts. I. P-V-T relations in the system $NaAlSi_3O_8$–H_2O to 10 kilobars and 1000°C. *Am. J. Sci., 270,* 54–79.

——— and ——— (1974) The role of H_2O in silicate melts. II. Thermodynamic and phase relations in the system $NaAlSi_3O_8$–H_2O to 10 kilobars, 700° to 1100°C. *Am. J. Sci., 274,* 902–940.

Chou, I-M. and R. J. Williams (1977) Activity of H_2O in CO_2–H_2O at 600°C and pressure to 8 kilobars (abstr.). *Geol. Soc. Am. Abstracts with Programs, 9,* 928.

Clark, S. P. (1966) Solubility. In S. P. Clark, Ed., *Handbook of Physical Constants,* p. 415–436. Geol. Soc. Am. Mem. 97.

Eggler, D. H. (1973) Effect of CO_2 on melting processes in the mantle. *Carnegie Inst. Wash. Year Book, 72,* 457–467.

——— (1977) Calibration of a Pyrex solid-media assembly. *Carnegie Inst. Wash. Year Book, 76,* 656–658.

——— and C. W. Burnham (1978) Activity of H_2O in diopside melt and CO_2–H_2O vapor to 20 kilobars, 600–1400°C (abstr.). *Geol. Soc. Am. Abstracts with Programs, 10,* 395.

———, I. Kushiro and J. R. Holloway (1979) Free energies of decarbonation reactions at mantle pressures: I. Stability of the assemblage forsterite–enstatite–magnesite in the system MgO–SiO_2–CO_2–H_2O to 60 kbar. *Am. Mineral., 64,* 288–293.

———, B. O. Mysen and T. C. Hoering (1974) Gas species in sealed capsules in solid-media, high-pressure apparatus. *Carnegie Inst. Wash. Year Book, 73,* 228–232.

——— and M. Rosenhauer (1978) Carbon dioxide in silicate melts: II. Solubilities of CO_2 and H_2O in $CaMgSi_2O_6$ (diopside) liquids and vapors at pressures to 40 kb. *Am. J. Sci., 277,* 64–94.

Goranson, R. W. (1938) Silicate–water systems: phase equilibria in the $NaAlSi_3O_8$–H_2O and $KAlSi_3O_8$–H_2O systems at high temperatures and pressures. *Am. J. Sci., Day Volume, 35A,* 71–91.

Holloway, J. R. (1977) Fugacity and activity of molecular species in supercritical fluids. In D. G. Fraser, Ed., *Thermodynamics in Geology,* p. 161–181. D. Reidel Publishing Company, Boston.

Kesson, S. E. and J. R. Holloway (1974) The generation of N_2–CO_2–H_2O fluids for use in hydrothermal experimentation. II. Melting of albite in a multispecies fluid. *Am. Mineral., 59,* 598–603.

Kracek, F. C. and K. J. Neuvonen (1952) Thermochemistry of plagioclase and alkali feldspars. *Am. J. Sci., Bowen Vol.,* 293–318.

Millhollen, G. L. (1971) Melting of nepheline syenite with H_2O and H_2O–CO_2 and the effect of dilution of the aqueous phase on the beginning of melting. *Am. J. Sci., 270,* 244–254.

———, P. J. Wyllie and C. W. Burnham (1971) Melting relations of $NaAlSi_3O_8$ to 30 kb in the presence of H_2O:CO_2 = 50:50 vapor. *Am. J. Sci., 271,* 473–480.

Mysen, B. O. (1976) The role of volatiles in silicate melts: solubility of carbon dioxide and water in feldspar, pyroxene, and feldspathoid melts to 30 kb and 1625°C. *Am. J. Sci., 276,* 969–996.

———, R. J. Arculus and D. H. Eggler (1975) Solubility of carbon dioxide in melts of andesite, tholeiite and olivine nephelinite composition to 30 kbar pressure. *Contrib. Mineral. Petrol., 53,* 227–239.

——— and M. G. Seitz (1975) Trace element partitioning determined by beta-track mapping; an experimental study with carbon and samarium as examples. *J. Geophys. Res., 80,* 2627–2636.

Robie, R. A. and D. R. Waldbaum (1968) Thermodynamic properties of minerals and related substances at 298.15°K (25°C) and one atmosphere (1.013 bars) pressure and at higher temperatures. *U. S. Geol. Surv. Bull. 1259.*

Roedder, E. (1970) Laboratory studies on inclusions in the minerals of Ascension Island granitic blocks, and their petrologic significance. In *Problems of Petrology and Genetic Mineralogy, V. S. Sobolev Memorial Volume II,* p. 247–258. Nauka Publishing House, Moscow.

Sobolev, V. S., I. T. Bakumenko, N. L. Dobretsov, N. V. Sobolev and V. V. Khlestov (1970) Physicochemical conditions of plutonic petrogenesis. (in Russian) *Geology and Geophysics, 124,* 25–35.

Touret, J. (1971) Le facies granulite en Norvege Meridionale. II. Les inclusions fluides. *Lithos, 4,* 423–436.

Yoder, H. S., Jr. (1950) High–low quartz inversion to 10,000 bars. *Trans. Am. Geophys. Union, 31,* 827–835.

Manuscript received, October 11, 1978;
accepted for publication, February 6, 1979.